Supplemental Procedures

S1 The Swift-Hohenberg model

The Swift-Hohenberg (SH) model (Equation 1 in the main text) is a well-studied phenomenological model of periodic patterning[1]. It represents a simple mathematical description of a Turing instability and encompasses many local activation, long-range inhibition models (and the corresponding local inhibition, long range activations models, such as the substrate-depletion model[2]). Whilst this equation cannot capture some aspects of more complex mechanisms (since it is only a one-variable model), it forms a good approximation in a parameter regime near the onset of Turing instability.

S1A The Swift-Hohenberg equation can qualitatively describe a more complicated set of PDEs near the onset of Turing instability

Imagine we have a generic set of PDEs (that is invariant under rotations and translations):

$$\frac{\partial A_i}{\partial t} = f_i\left(\{A_j, \nabla^2 A_j, \nabla^4 A_j..\}_j\right) \tag{S.1}$$

where $\{A_j\}$ are the variables in the system. If we assume that we are near the onset of a Turing instability i.e. instability of the homogeneous steady state, we can consider deviations of equation S.1 about the steady state. This separates the equation into a linear component that dominates the behaviour for small disturbances, and a stabilizing nonlinear term:

$$\frac{\partial \delta A_i}{\partial t} = \sum_j \mathcal{M}_{ij}\delta A_j + g_i(\{\delta A_j\}_j) \tag{S.2}$$

We can then diagonalize the operator $\mathcal{M}$ and transform from the basis $\{A_j\}$ to the diagonal basis, $\{\phi_j\}$. In this case, the matrix dependence of the linear term disappears:

$$\frac{\partial \phi_i}{\partial t} = \mathcal{M}_{ii}\phi_i + g_i(\{\phi_j\}_j) \tag{S.3}$$

In the case that only a single mode exhibits a Turing instability, the other modes will rapidly decay to zero (i.e. $M_{ii}\phi_i < -k\phi_i$ for some positive k, for all ϕ_i). Consequently we can consider just one equation of the set described by equation S.3. Denoting the Turing-unstable mode by ϕ, we can write:

$$\frac{\partial \phi}{\partial t} = \mathcal{M}\phi + g(\phi) \tag{S.4}$$

Assuming that $\mathcal{M}$ is translationally and rotationally invariant means that $\mathcal{M}_{\mathbf{q}}$ is a function of $\mathbf{q}^2$. Expanding about the $|\mathbf{q}| = 0$ long wavelength limit, we arrive at $\mathcal{M}_{\mathbf{q}} = \alpha + \beta|\mathbf{q}|^2 + \gamma|\mathbf{q}|^4$, where α, β, γ are constants. Note that all three terms are required to describe a pattern that has a Turing instability over a finite set of wavelengths[1]. Reparameterizing this expansion identifies $\mathcal{M}_{\mathbf{q}} \equiv a - \mathcal{L}_{\mathbf{q}}$ in the Swift-Hohenberg model.

The specific form of the nonlinearity $g(\phi)$ is left unspecified. Near the onset of Turing instability, we expect the pattern amplitude to be small, and thus can expand $g(\phi) \approx -c\phi^2 - d\phi^3$. If in addition, we require that the steady state pattern is stripes, not spots, and follow the analysis of [3] and simulations of [4], and set $c = 0$ to favour exclusively striped patterns.

To summarize, if we take a set of PDEs and (i) expand about a homogeneous steady state, (ii) assume a single mode exhibits a Turing instability, (iii) assume that we are in a regime near the onset of the instability, and (iv) assume the pattern is exclusively striped, then we can motivate an equation qualitatively similar to the Swift-Hohenberg equation. This formalizes the idea that many different PDEs can be qualitatively described by a simple, generic equation, at least in certain limits. Outside of these limits the formal mapping no longer holds, however in nonlinear systems the limits can often describe behaviours in other regimes[1].

S1B The Swift-Hohenberg operator, $\mathcal{L}$, is associated with local activation, long-range inhibition (LALI)

To illustrate the intuition behind $\mathcal{L}$, we use an example - model #3 in section S10. Here, the dynamics of the differentiation status of the cells, $\phi(\mathbf{x}, t)$ is described by an equation of the form:

$$\frac{d\phi}{dt} = K * \phi \tag{S.5}$$

[1] An alternative way to motivate this is to require $\mathcal{M}_{\mathbf{q}} > 0$ for some small regime near $\mathbf{q}_0$, i.e. a form $\mathcal{M}_{\mathbf{q}} \sim A - B(q^2 - q_0^2)^2$, which is equivalent to the expression above

where $*$ denotes the convolution operator and K is an interaction function. In general, K describes the LALI interaction (or vice versa, the LILA interaction); for model #3, for simplicity in 1D, this is of the form:

$$K(\mathbf{x}) = K_A e^{-|\mathbf{x}|/L_A} - K_I e^{-|\mathbf{x}|/L_I} \tag{S.6}$$

To see the correspondence to the Swift-Hohenberg equation, we fourier transform equation S.5 and equation 1 and can immediately make the following identification:

$$K_{\mathbf{q}} \leftrightarrow a - \mathcal{L}_{\mathbf{q}} \tag{S.7}$$

Does this assignment hold? In figure S1, we plot the two expressions as a function of q and find that, near the onset of Turing instability, the Swift-Hohenberg expression, $\mathcal{L}_{\mathbf{q}}$, provides a reasonable approximation to the actual interaction function, $K_{\mathbf{q}}$. We expect this to hold for a variety of interaction functions, but again only in the limit near the onset of Turing instability.

Thus, the operator $\mathcal{L}$ is intimately linked to the nonlocal interactions in the system, and can be viewed as an approximate description of a range of different LALI interactions.

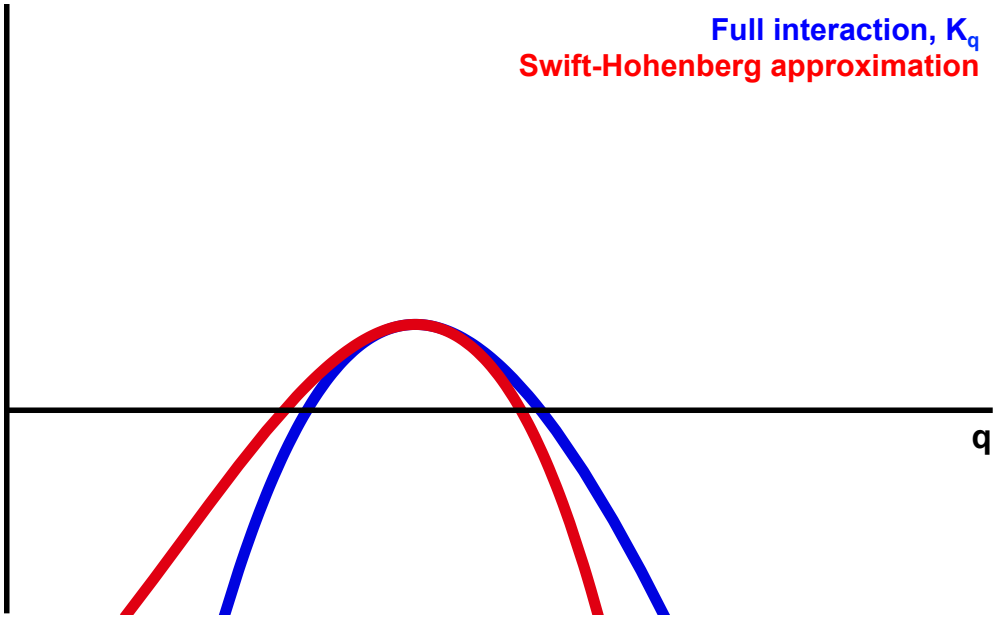

Figure S1: A comparison of the interaction function, $K_{\mathbf{q}}$, with the approximation by the Swift-Hohenberg equation reveals that $a - \mathcal{L}_{\mathbf{q}} \approx K_{\mathbf{q}}$ for suitable parameters near the onset of a Turing instability. Related to Fig. 1

S1C Where does the Swift-Hohenberg approximation fail?

The model we use describes stripes formed by a Turing instability. This excludes the formation of non-striped patterns (e.g. spots, or graded transitions from spots to stripes) but also excludes stripes formed by a non-Turing mechanism e.g. pair rule gene expression in early Drosophila patterning[5]. A potentially more confusing case is where a Turing instability is present, but is accompanied by other instabilities. In this case, our theory also breaks down. We illustrate this with two examples.

First, a number of reaction-diffusion models have been shown to display travelling wave behaviour (in addition to a Turing instability). We find that, in this case, a parameter gradient can generate travelling waves and orient stripes perpendicular to the gradient, see figure S2A and also the results from [4].

Second, reaction-diffusion models can also exhibit oscillatory dynamics. Again, a parameter gradient can have nontrivial consequences on an oscillating + Turing system. In some regimes, stripes can form perpendicular to the gradient, provided the gradient transitions the system from an oscillatory to a Turing state (see figure S2B).

Thus in both these cases, our model for stripe orientation does not apply. The reason is that our model applies to a qualitatively different process, excluding both oscillations and travelling waves. However, simple observation of the patterning process *in vivo* can dictate which of these qualitative models is appropriate. For example, neither travelling waves nor oscillations are seen during digit/non-digit patterning, suggesting that the Swift-Hohenberg formulation is appropriate.

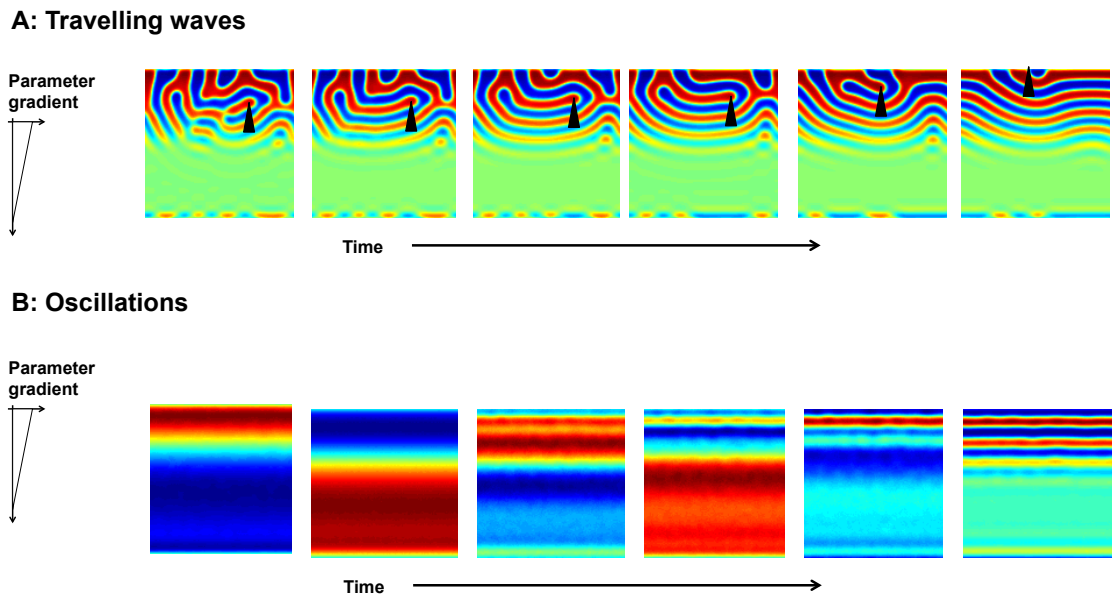

Figure S2: A: Using the model described by equation S.42, a parameter gradient in f_V can orient stripes perpendicular to the gradient. The dynamics of orientation involves travelling waves (arrowhead highlights the travelling behaviour of a certain portion of the pattern). B: Using the model described by equation S.40, a parameter gradient can orient stripes perpendicular to the gradient by producing synchronized oscillations. Related to Fig. 3

S2 Simulations

S2A Simulation methods

Equation 17 was simulated using a custom MATLAB script, available upon request. We simplified the core SH equation by moving to dimensionless variables as:

$$\frac{\partial \phi}{\partial t} = a\phi - (\nabla^2 + 1)^2\phi - \phi^3. \tag{S.8}$$

Equation S.8 was simulated on a 128×128 square grid in MATLAB (corrresponding to a physical length $L = 10\lambda$ i.e. $\sim$10 stripes.) We began each simulation with a set of different stochastic initial conditions (random numbers drawn from a normal distribution). The dynamics were solved using an algorithm that was inspired from an existing, freely available script [2] that transforms Equation S.8 into Fourier space in order to solve it (and thus uses cyclic boundary conditions). To examine the solution, we plotted $\phi(\mathbf{x}, t)$ as a RGB heatmap over time. For the figures in the main text, we plot the solution at a time $100a^{-1}$, which corresponded to a time where the pattern had almost stopped changing[3]. The results of each simulation vary due to the variable initial conditions. We therefore repeated each simulation a number of times to ensure the behavior that we observed was consistent.

S2B Parameter values

Equation S.8 has a single parameter, a, which we held constant for most of the simulations in the main text, $a = 0.1$ (the exceptions being figure 1A upper right, $a = 1.0$; S5A where $a = 0.1, 0.3, 1.0$ respectively; and lower right where $a = 0.01$.). For each of the simulations, we then modified Equation S.8 to resemble Equation 17, and we list the simulation details in the table below.

Table S1: Simulation details and parameter values for the results in the main text

Mechanism to orient stripes	Figure	Parameter values and implementation
Production gradient	2A	A linear gradient along the x-axis from $+h$ to $-h$ was added in the tissue, with $h = 0.0, 0.004, 0.01$
Parameter gradient	2B	$a(x)$ varied linearly from 0.1 to $-h$, with $h = -0.1, 0, 0.1$
Tissue anisotropy	2C	Operator $\mathcal{L}$ changed to $\mathcal{L} = (\nabla^2 + 1)^2 - h\partial_x^2$, with $h = 0, 0.01, 0.5$
Anisotropic growth	2D	Pattern was 'grown' at each timestep via $\phi(x, y, t + \delta t) = \phi(x/(1 + h\delta t), y, t)$. with $h = 0, 0.05, 0.1$

S2C Stripes may be oriented despite variability in initial conditions

To investigate the dependence of stripe orientation on initial conditions, we varied the initial conditions in our simulations. Firstly, we used 'stochastic' initial conditions, in which each spatial gridpoint has a normally distributed random number as its initial condition. We chose the standard deviation of this distribution to be roughly equal to the final pattern amplitude. We then repeated the simulation many times and observed the variability in stripe direction.

To quantify the variability in stripe direction, we wrote a script to measure stripe angle by computing the pattern fourier transform and looking for the dominant modes (figure S3A). We then represent the stripe direction on a polar plot, where the polar angle corresponds to the angle of the stripes. For each of the mechanisms in the main text, we repeated the simulation 100 times, for a number of parameter sets, and plotted the distribution of final stripe direction. As expected, for parameter sets that are weakly orienting, variable initial conditions can result in variable final patterns. However, we see that as the orientation mechanism increases in magnitude, that stripes may be robustly oriented despite variability in initial conditions (figure S3B).

The extreme of this would be starting from A-stripes and evolving to B-stripes, or vice versa. The analysis of section S6-9 predicts that, under some parameter regimes, instability of A-stripes is certainly possible. Indeed, when using A stripes as initial conditions, we could observe instability of these stripes when an orientation mechanism was present that tended to favour B stripes, and vice versa (see figure S4).

[2] written by Roman Gregoriev and modified by Karen Daniels *http://nile.physics.ncsu.edu/hon292a-f08/*

[3] We choose to plot this timepoint, as opposed requiring the solution to converge, in order to show the different strengths and/or speeds between the different orientation mechanisms

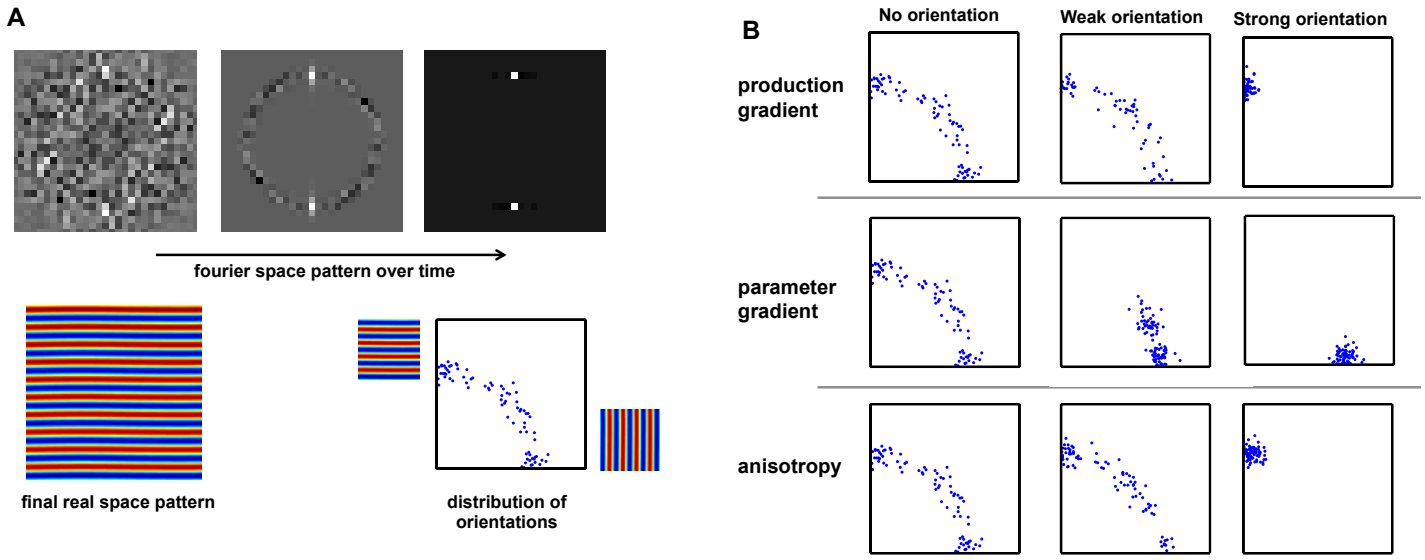

Figure S3: A: Upper: By Fourier transforming striped patterns and finding the dominant wavevector, we may infer stripe orientation from simulation results. Each simulation is plotted as a polar angle over $\pi/2$ of the unit circle, with random scatter added to distinguish identical angles. Lower: Stripes are randomly oriented in the absence of orientation mechanisms. B: Depending on the strength of each orientation mechanism, stripes may be unoriented, weakly oriented or strongly oriented, even in the presence of variable initial conditions. Related to Fig. 2.

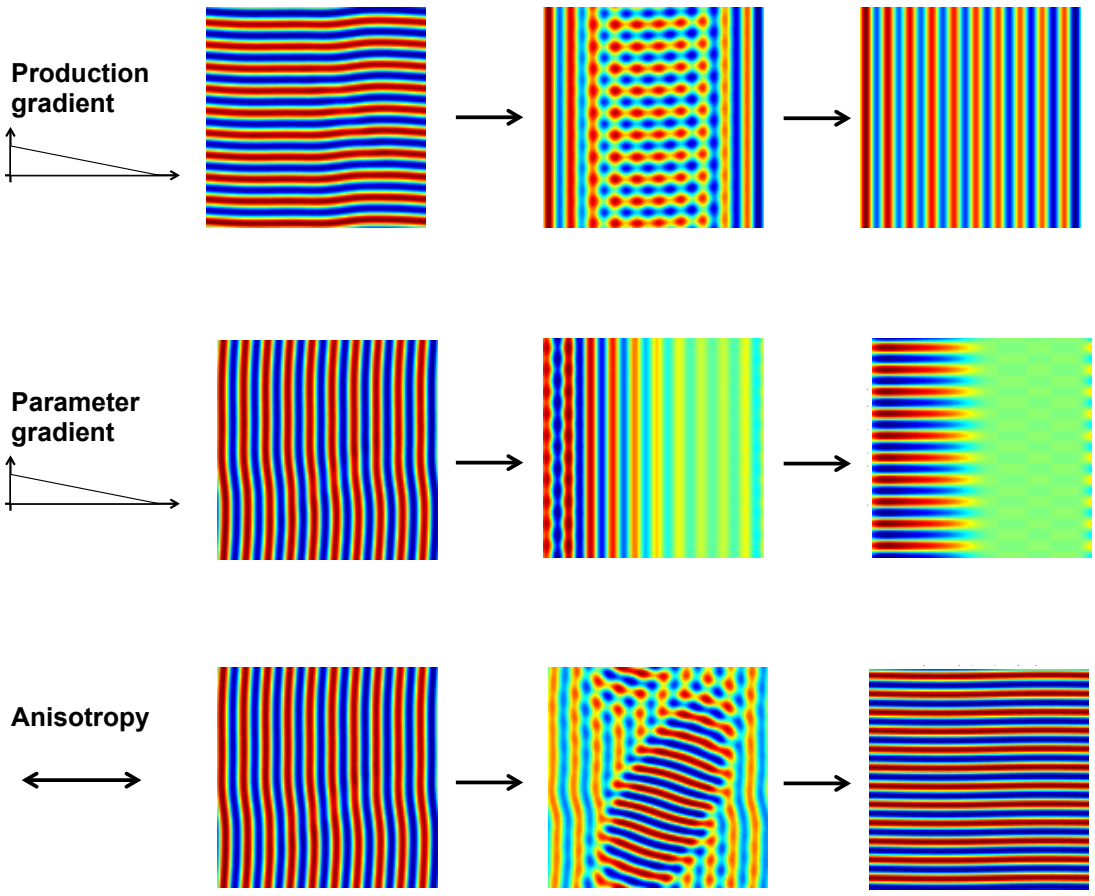

Figure S4: In some parameter regimes, stripe orientation is sufficiently strong to completely reorient stripes. Related to Fig. 2.

S3 Defining pattern orientation

The orientation of periodic patterns is often parameterized by a wavevector, $\mathbf{q}$, that specifies the direction and spacing of the pattern, see Figure 1 of the main text. (Spotted patterns can be considered as superpositions of periodic solutions with different wavevectors, e.g. in a hexagonal lattice, these wavevectors are rotated $\pi/3$ w.r.t. one another[6]).

There are two ways that stripe direction can be variable: 1) stripe direction can vary across space within a tissue (Figure S5A), and 2) stripe direction is constant in space, but varies due to stochastic effects, often variable initial conditions (Figure S5B). In this work we choose a parameter regime where the stripes are largely straight ($a \to 0$) but the direction of the stripes is random in the absence of other factors (like Figure S5B).

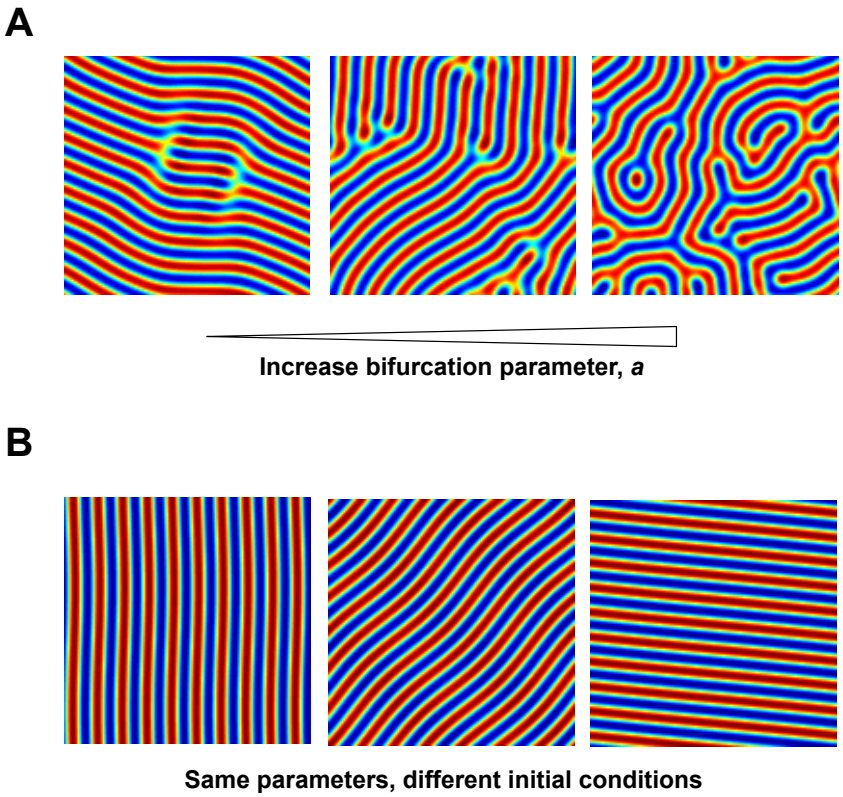

Figure S5: A: Increasing the parameter a reduces the 'straightness' of stripes, so that stripe direction varies continuously across space within the tissue. B: Even for 'straight stripes' ($a = 0.01$), randomly seeded initial conditions generate stripes with different orientations. Related to Fig. 2.

S4 Stripes oriented by an arbitrary angle

In the main text we have focussed on two possible stripe orientations - vertical A stripes and horizontal B stripes. Here we will argue that by considering just these two stripe orientations, we may infer the general behavior of stripe orientation.

For concreteness, consider an orientation mechanism (gradient or anisotropy) that is directed along the x-axis. Now, by symmetry, the stripes will have a tendency to align along the y-axis (A stripes) or along the x-axis (B stripes). To illustrate the logic, we first choose a mechanism that generates B-stripes. We then wish to ask: what range of other possible stripe orientations exist?

To answer this question, we consider A_θ-stripes, oriented at an angle θ w.r.t. B-stripes (Figure S6A). In the main text, we derived amplitude equations for the case $\theta = \pi/2$, and quantified each in terms of a parameter p that introduced asymmetry between A- and B-stripes (where p could be one from the set $\{h_A, \alpha, \Delta r \equiv r_A - r_B\}$). Stripe orientation arose when p increased past a critical value p_{crit}. Now, these parameters can also be calculated for A_θ stripes - specifically $p \equiv p(\theta)$ takes on an angular dependence. Whilst the precise form of this dependence may be complicated, we have: 1) $p(\theta = 0) = 0$; and 2) $p(\theta)$ is monotonically increasing over $(0, \pi/2]$. Thus, when considering the alignment of B-stripes, we have the following three regimes (figure S6B):

1. No stripe orientation, $p_{\pi/2} \ll p_{\text{crit}}$
2. Some stripe orientation, $p_{\pi/2} \sim p_{\text{crit}}$

3. Strong stripe orientation, $p_{\pi/2} \gg p_{\text{crit}}$

Therefore, by analyzing the case $\theta = \pi/2$ we determine the transition from randomized stripes to weakly oriented stripes. Then, by using this, and by the monotonicity of $p(\theta)$, we can deduce the qualitative behavior of arbitrarily oriented stripes A_θ - as the stripe orientation effect becomes stronger, a narrower range of stable stripe orientations is admissible.

This result can be generalized to write amplitude equations for two arbitrarily aligned stripes: A_θ, A_ϕ. Again, we deduce that the parameter p that describes the asymmetry between A_θ, A_ϕ, will be extremized for: 1) θ, ϕ separated by $\pi/2$, and 2) θ or ϕ are along the x-axis (the direction of the orientation mechanism, via symmetry). In this case, either A or B stripes will be most stable and selected for large values of p. The qualitative behavior (i.e. classifying the mechanism as either A or B in figure S6B,C) can be determined by considering perpendicular A- and B-stripes only, thus motivating the analysis in the main text.

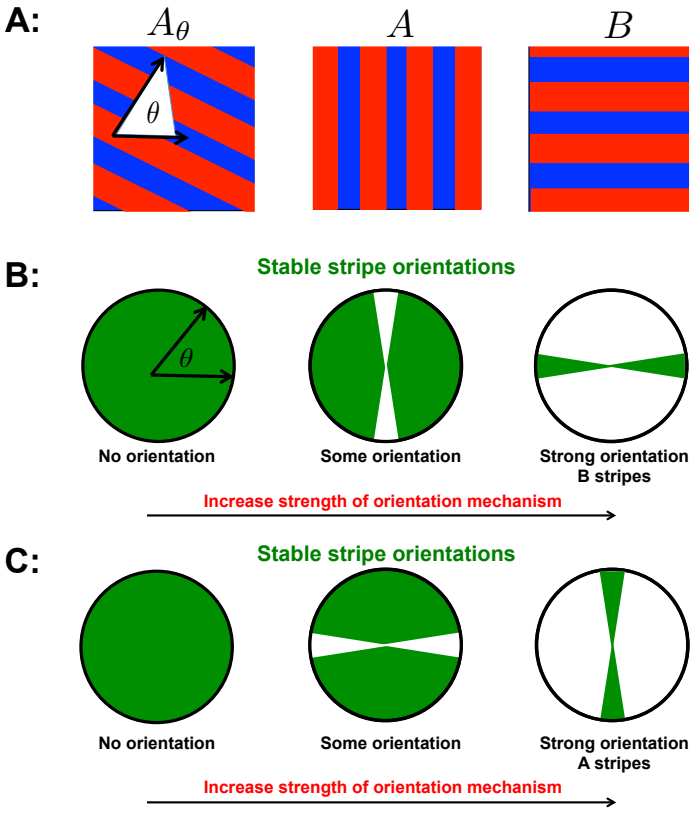

Figure S6: A: Schematic of A_θ, A and B stripes. B: Qualitative behavior of B stripes. As the orientation mechanism increases in strength, the region of stable stripe orientations (green) narrow. On the far right is an example of strongly oriented B stripes. C: Same as above, but for A stripes. Related to Fig. 2.

S5 Deriving amplitude equations

To understand how periodic patterns are oriented, we look for steady state solutions of Equation 1. In the limit $a \to 0$, these steady state solutions can be approximated as linear superpositions of functions of the form:

$$A(\mathbf{x},t)\mathrm{e}^{i\mathbf{q}.\mathbf{x}} + A^*(\mathbf{x},t)\mathrm{e}^{-i\mathbf{q}.\mathbf{x}}, \tag{S.9}$$

with $|\mathbf{q}|^2 = q_0^2$, and $\theta \equiv \cos^{-1}(\mathbf{q}.\hat{\mathbf{i}})/q_0$ is the angle the pattern makes with the x-axis. The problem of pattern orientation is then reduced to understanding which of these function(s) are a **stable** steady state solution of Equation 1?

To determine this we perform a bifurcation analysis of Equation 1, following the approach of e.g. [6, 7, 8, 9, 10]. In particular, we explore the equation near the onset of Turing instability, by setting $a \to \epsilon^2 a$, where ϵ is the bifurcation parameter. We consider slowly varying variations in the amplitude of periodic solutions to Equation 1, by defining a timescale T as $\partial_t = \epsilon^2 \partial_T$. Performing a bifurcation analysis, we write:

$$\phi = \epsilon\phi_0 + \epsilon^2\phi_1 + \epsilon^3\phi_2. \tag{S.10}$$

Equating terms of order ϵ and ϵ^2 gives $\mathcal{L}\phi_0 = \mathcal{L}\phi_1 = 0$, i.e. periodic solutions with wavevector $|\mathbf{q}|^2 = q_0^2$. The amplitude equation is generated from the ϵ^3 term, giving:

$$\mathcal{L}\phi_2 = a\phi_0 - d\phi_0^3 - \dot{\phi_0}. \tag{S.11}$$

Since $\mathcal{L}\phi_0 = 0$, the RHS and LHS of Equation S.11 are orthogonal, hence must be identically zero, giving:

$$\dot{\phi_0} = a\phi_0 - d\phi_0^3. \tag{S.12}$$

Substituting the ansatz

$$\phi_0 = A(\mathbf{x},t)\mathrm{e}^{iq_0x} + A^*(\mathbf{x},t)\mathrm{e}^{-iq_0x} + \tag{S.13}$$
$$+B(\mathbf{x},t)\mathrm{e}^{iq_0y} + B^*(\mathbf{x},t)\mathrm{e}^{-iq_0y}, \tag{S.14}$$

(which satisfies $\mathcal{L}\phi_0 = 0$) we arrive at the equation:

$$\dot{A} = aA - 3d|A|^2A - 6d|B|^2A, \tag{S.15}$$

and vice versa for B. Therefore, we arrive at Equations 4,5 if we rescale the time units and identify $r = a/3d$.

To understand why stripes are the only stable solution for this equation, we consider the alternative of a square array of spots, i.e. $A = B$. In this case, the steady state solutions of Equations 4,5 give $|A|^2 = r/3$, and disturbances about this steady state are governed by the equations:

$$\frac{\partial}{\partial t}\begin{pmatrix}\delta A\\ \delta B\end{pmatrix} = -\frac{2r}{3}\begin{pmatrix}1 & 2\\ 2 & 1\end{pmatrix}\begin{pmatrix}\delta A\\ \delta B\end{pmatrix}, \tag{S.16}$$

which can easily be shown to be unstable.

We now consider the effect of each of the orientation mechanisms considered in this article. The approach in each case follows that of above: 1) perform a bifurcation analysis, 2) derive amplitude equations, 3) solve for the steady states, and 4) determine the stability of these steady states.

S6 Production gradient

We modify Equation 1 to include the effects of a spatially varying production in the pattern variable, i.e.

$$\frac{\partial\phi}{\partial t} = a\phi - \mathcal{L}\phi - d\phi^3 + h(\mathbf{x}). \tag{S.17}$$

Again, we use a bifurcation expansion to derive the amplitude equations. The relevant scaling for h that describes its effect on the stability of periodic patterns (as opposed to it dominating the patterning) is $a \to \epsilon^2 a$, $h \to \epsilon^3 h$. This generates a modified version of Equation S.12:

$$\dot{\phi_0} = a\phi_0 - d\phi_0^3 + h. \tag{S.18}$$

To substitute ansatz S.14 into Equation S.18, we require the Fourier representation of the gradient:

$$h(\mathbf{x}) = \sum_{\mathbf{q}} h_{\mathbf{q}} \mathrm{e}^{i\mathbf{q}.\mathbf{x}} + h_{\mathbf{q}}^* \mathrm{e}^{-i\mathbf{q}.\mathbf{x}}. \tag{S.19}$$

Assuming that the gradient is along the x-axis (h is a function of x alone), then we may identify:

$$\dot{A} = aA - 3d|A|^2A - 6d|B|^2A + h_{\mathbf{q}=(q_0,0)}, \tag{S.20}$$

with the h term absent in the equivalent equation for B. We may assume a form for $h(x)$ to calculate the magnitude of the additional term, e.g. $h(x) = h_0 \exp[-|x|/l]$ gives $h_{\mathbf{q}=(1,0)} = 2h_0 q_0 l(1 + q_0^2 l^2)^{-1}$. Redefining constants recasts the equation into Equations 9,10.

To solve the for the solutions of Equations 9,10 and their stability, we consider the nullclines $\dot{A} = \dot{B} = 0$. $B = 0$ is a trivial stable solution, corresponding to stripes aligned along the y-axis. The second stable solution, corresponding to $A = 0$ for $h = 0$ loses stability when the nullclines no longer intersect. This is solved by writing the nullclines as:

$$B^2 = r - 2A^2, \tag{S.21}$$

$$B^2 = \frac{1}{2}(r - A^2 + \frac{h}{A}) \tag{S.22}$$

By equating these two functions, and their derivatives, we arrive at a critical value for h as described in the main text.

S7: Parameter gradient

For the case of an parameter gradient, we modify Equation 1 to include spatial variation in parameters. Accordingly, when performing a bifurcation analysis of this equation, we must consider not only variations in amplitude over time, but also variations over space. Letting X and Y denote slow spatial variations, and T slow time variations, we can rewrite the bifurcation transformations as: $a \to \epsilon^2 a$, $\partial_t = \epsilon^2 \partial_T$ and $\nabla \to \nabla + \epsilon\tilde{\nabla}$, where $\nabla \equiv (\partial_x, \partial_y)^T$ acts on the rapidly varying, periodic functions of the form $\exp[i\mathbf{q}.\mathbf{x}]$, and $\tilde{\nabla} \equiv (\partial_X, \partial_Y)^T$ corresponds to the slow amplitude variations. When applied to the operator defined in Equation 2, we obtain:

$$\mathcal{L} \to \mathcal{L}_\epsilon = a\kappa \left(q_0^{-2}(\nabla + \epsilon\tilde{\nabla})^2 + 1 \right)^2. \tag{S.23}$$

Considering the ϵ and ϵ^2 expansion terms gives $\mathcal{L}\phi_0 = \mathcal{L}\phi_1 = 0$ as before. The effect of the spatial fluctuations appears in the ϵ^3 term, generating the amplitude equation:

$$\dot{\phi_0} = a\phi_0 - d\phi_0^3 + 4a\kappa q_0^{-4}(\nabla.\tilde{\nabla})^2\phi_0. \tag{S.24}$$

If we substitude ansatz S.14 into this equation, we obtain:

$$\dot{A} = r(X,Y)A - |A|^2A - 2|B|^2A + \alpha A_{XX}, \tag{S.25}$$

$$\dot{B} = r(X,Y)B - |B|^2B - 2|A|^2B + \alpha B_{YY}, \tag{S.26}$$

wtih α a constant defined as $\alpha \equiv 4a\kappa/3dq_0^2$. For parameter variations purely along the x-axis, the Y dependence vanishes, and we arrive at Equations 12,13, where we have dropped the capitalization for convenience in the main text.

To solve these equations, we focus on a regime near the onset of Turing instability $r \to 0$, such tht $r(x)$ changes sign in the patterning field (Figure S7A)[6]. This is likely a relevant scenario *in vivo* - the position where $r(x)$ changes sign controls the boundary where the periodic pattern begins. For example, the murine limb bud has been proposed to transition from a non-Turing regime (the forearm) to a Turing regime (the digits) via a proximal-distal gradient of *hoxd13*[11, 4] (Figure S7B).

In this scenario, close to the gradient source, the pattern will be described by either $(A, B) = (\sqrt{r_\infty}, 0)$ or $(A, B) = (0, \sqrt{r_\infty})$. Far away from the gradient we are below the Turing instability threshold and thus $(A, B) = (0, 0)$. To determine

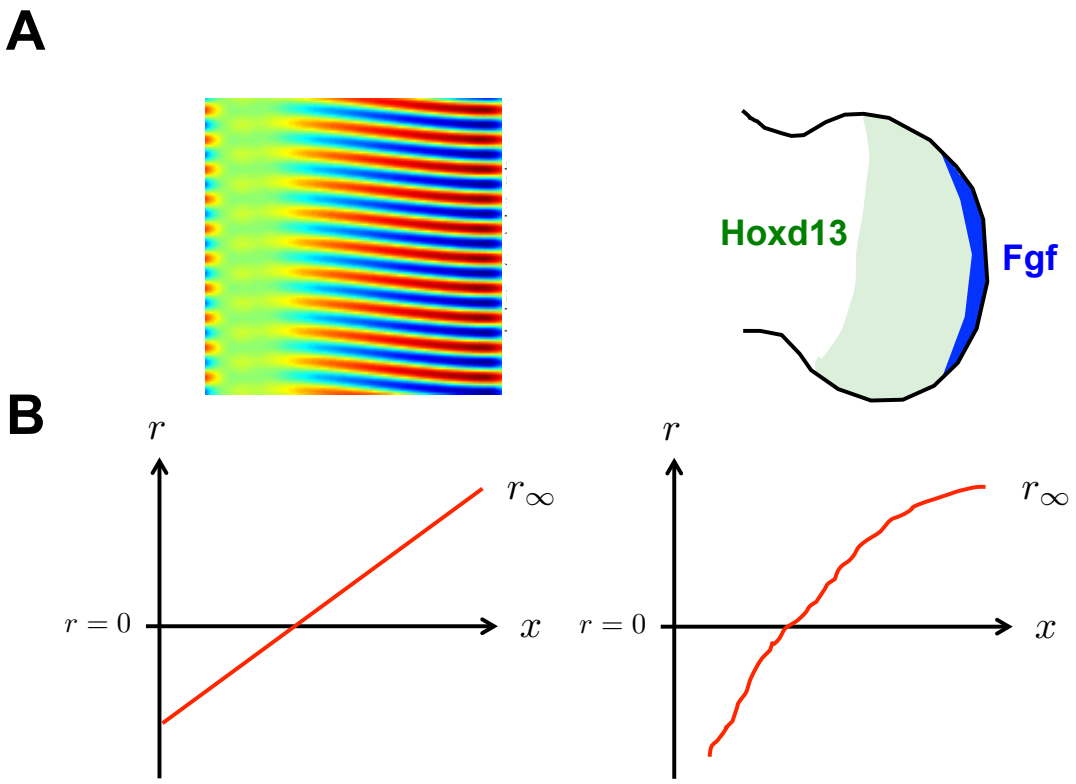

Figure S7: A parameter gradient from sub-Turing to Turing regimes. A: Transition to a Turing regime in simulation (left) and in a schematic of limb development (right). B: Proposed parameter values as a function of distance, $r(x)$, for the two cases above. Related to Fig. 2.

the stability of each stripe direction we focus on the transition region. One possible steady state solution is $B = \sqrt{r(x)}$, $A = 0$. Variations about this steady state are described by equations:

$$\delta\dot{A} = -r(x)\delta A + \alpha\delta A_{xx}, \tag{S.27}$$

$$\delta\dot{B} = -2r(x)\delta B, \tag{S.28}$$

i.e. this solution is a stable steady state. In contrast, consider the steady state with $B = 0$. Equation S.26 implies continuity of A and $\partial A/\partial x$ in space. Therefore, near the onset of instability, defined by $r(x_0) = 0$, A increases from zero to $\sqrt{r_\infty}$, but in a way that respects the continuity of A and $\partial A/\partial x$, i.e. $A \propto (x - x_0)^2$ near x_0. Now, consider the fluctuations in the amplitude B about this steady state:

$$\delta\dot{B} = (r(x) - 2|A|^2)\delta B. \tag{S.29}$$

Since $r(x)$ near the transition will be linear in space, $r(x) \sim x - x_0$, whereas $A(x) \sim (x - x_0)^2$, then for sufficiently small $x - x_0$, this steady state will become unstable to patterns in the transverse direction. Putting these results together mean that $(A, B) = (0, \sqrt{r(x)})$ is the stable solution of Equation 11, i.e. parameter gradients can orient stripes **parallel** to the gradient[4]

S8 Tissue anisotropies

In an isotropic and translationally invariant system, the operator $\mathcal{L}$ in Equation 1 takes a particular form. Specifically, the Fourier transform, $\mathcal{L}_\mathbf{q} \equiv \mathcal{L}_\mathbf{q}(|\mathbf{q}|^2)$ is a function of wavevector magnitude only. In an anisotropic (but translationally invariant) system, this restriction changes to $\mathcal{L}_\mathbf{q} \equiv \mathcal{L}_\mathbf{q}(q_x^2, q_y^2)$. In this case, the relevant Turing instability parameter, a, will take different values according to the direction of the stripes. For stripes along the x-axis, $a_X = a - \min_{q_0}\mathcal{L}_\mathbf{q}(q_0^2, 0)$, and for stripes along the y-axis $a_Y = a - \min_{q_0}\mathcal{L}_\mathbf{q}(0, q_0^2)$. If $a_X \neq a_Y$, then the system is anisotropic. Applying these relations to Equation S.12 and ansatz S.14 generates Equations 15,16 in the main text:

[4]The effective strength of this orientation can be rationalized by considering the size of the parameter α. By dimensional analysis, this sets a lengthscale $l \sim \sqrt{\alpha/r} \sim \frac{\sqrt{\kappa}}{\pi}\lambda$ that determines over what distance this effect will be realized. For small α, the effect will be moderate; whereas the effect will become prominent as α increased.

$$\dot{A} = r_A A - |A|^2 A - 2|B|^2 A, \tag{S.30}$$
$$\dot{B} = r_B B - |B|^2 B - 2|A|^2 B. \tag{S.31}$$

Consider the steady state $(A, B) = (0, \sqrt{r_B})$. Fluctuations about this steady state obey the equations:

$$\delta\dot{A} = (r_A - 2r_B)\delta A \tag{S.32}$$
$$\delta\dot{B} = -2r_B \delta B, \tag{S.33}$$

i.e. this steady state is stable if $r_A < 2r_B$, and vice versa for the solution $(A, B) = (\sqrt{r_A}, 0)$. Putting this together means that, for $r_B > 2r_A$, then 1) B stripes are stable *and* 2) A stripes are unstable, as reported in the main text. Thus, parameter anisotropies in the tissue can orient stripes, in the direction that maximizes the Turing instability parameter, r (Figure 2C).

S9 Anisotropic growth

We consider two types of growth. The first type is tissue growth *without* pattern growth. An example of this would be a reaction-diffusion system where the tissue grows via cell division. As the tissue grows, the effective concentration of the reaction-diffusion molecules will be continuously diluted. In contrast, a second case is where tissue growth occurs *with* pattern growth. For example, in a cell-based mechanism, cell growth naturally involves replication of the pattern - since growth is driven by cell division. Note, a third type of growth that has been considered elsewhere is growth where material is simply added to the boundary of the tissue, see [12].

In both these cases, the growth generates an effective flow field (or velocity) in the tissue, $\mathbf{v}(\mathbf{x}, t)$, related to the local growth rate $g(\mathbf{x}, t)$ via $\nabla.\mathbf{v} = g$[13]. For example, uniform growth directed along the x-axis generates a flow field $\mathbf{v} = gx\mathbf{i}$.

For case 1 (tissue growth *without* pattern growth), this flow has two consequences: advection and dilution. This is summarized by adding a term $-\nabla.(\mathbf{v}\phi)$ to Equation 1[14]. Noting that $\nabla.\mathbf{v} = g$, we arrive at:

$$\frac{\partial\phi}{\partial t} = (a - g)\phi - \mathcal{L}\phi - d\phi^3 - \mathbf{v}.\nabla\phi. \tag{S.34}$$

The term $-g\phi$ represents dilution - note that fast growth can drive the system below the Turing regime via this dilution.

In case 2 (tissue growth *with* pattern growth), the dilution is absent, i.e. we have:

$$\frac{\partial\phi}{\partial t} = a\phi - \mathcal{L}\phi - d\phi^3 - \mathbf{v}.\nabla\phi. \tag{S.35}$$

Thus the two types of growth can be mapped onto one another provided we rewrite $a \to a + g$ for case 1.

To model anisotropic growth we consider the extreme of growth along the x-direction, i.e. $\mathbf{v} = v_x\mathbf{i}$. As before, we perform a bifurcation analysis of Equation S.35. Since $\mathbf{v}$ is a velocity, and since $\partial_x \to \epsilon\partial_X, \partial_t \to \epsilon^2\partial_T$ from before, we have that $v \to \epsilon v$. Substituting Equation S.10 into Equation S.35 and equating terms of order ϵ^3 yields:

$$\dot{\phi_0} = a\phi_0 - d\phi_0^3 - v\frac{\partial\phi_0}{\partial x}. \tag{S.36}$$

Using the ansatz S.14, we obtain:

$$\dot{A} = aA - 3d|A|^2 A - 6d|B|^2 A - ivq_0 A, \tag{S.37}$$
$$\dot{B} = aB - 3d|B|^2 B - 6d|A|^2 B, \tag{S.38}$$

or, rewriting parameters:

$$\dot{A} = (r - i\beta)A - |A|^2 A - 2|B|^2 A, \tag{S.39a}$$
$$\dot{B} = rB - |B|^2 B - 2|A|^2 B, \tag{S.39b}$$

where $\beta \equiv vq_0/3d$ can vary across space, $\beta \equiv \beta(x)$.

Now, by looking for steady state solutions of Equation S.39, the imaginary term means that the steady state $B = 0$ is no longer admissible. In contrast, the steady state $(A, B) = (0, \sqrt{r})$ still exists and, analogously to Equation S.33, is a stable solution. Thus, stripes are oriented along the direction of maximal tissue growth.

We can also estimate the typical growth rates for which this effect is observed, by requiring $\beta \sim r$ to be of similar magnitude. This corresponds to $v \propto gL \sim a/q_0$, where L is the typical tissue size. Thus, for $g \ll a/q_0 L$, the effect of growth is negligible.

S10 Stripe orientation is qualitatively similar in a range of different periodic patterning mechanisms

S10A Applying our results to a canonical reaction-diffusion model

Whilst the existence of a bona fide reaction-diffusion model in biology is still debated, there are a number of chemical systems that can self-assemble into stripes. One such system is the CIMA reaction - one of the first experimental realizations of a Turing system - which involves the diffusion and reactions of chlorite-iodide and malonic acid[15]. Mathematical representations of this chemistry are well established, and we follow the Lengyel-Epstein model[16, 17] (detailed below).

Now, we wish to ask whether the results outlined in the main text hold for this system, and thus interrogate the generality of our results. We implement the model as a set of two-variable PDEs in MATLAB, on the same spatial domain as used for the Swift-Hohenberg model. We chose a parameter regime that gives striped patterns (as opposed spots, or labryinthine patterns), and then add one of a production gradient, a parameter gradient, or an anisotropy. In each case, we find that stripe orientation is qualitatively similar to the predictions from a Swift-Hohenberg model.

We refer back to section S1C to highlight some exceptions to the rule. In particular, the CIMA reaction can also exhibit oscillations and, if a parameter gradient moves the system into the oscillatory state, orientation by oscillation is possible, as in figure S2B. Similarly, some parameter gradients do not transition the system from a sub-Turing to a Turing state, and in this case stripe orientation is also not predicted by our model (e.g. if the transition is from a spotted to a striped state). Both the cases are qualitatively distinct from the 'parameter gradient' outlined in the main text, where the parameter concerned controls the onset of a Turing instability.

S10B Applying our results to other Turing models

We repeated the same type of analysis for several different Turing models - spanning molecular, cellular and mechanical processes - as shown in Figure 3 of the main text. The models we consider are:

1. A 2-component reaction-diffusion equation, consisting of an unspecified activator/inhibitor pair, as used in Sheth et. al. [4] to describe limb patterning.
2. A 3-component reaction-diffusion equation, consisting of two diffusible factors (BMP, Wnt) and a transcription factor (Sox9), used by Raspopovic et al. [11] to describe limb patterning.
3. A cell-based model, in which the differentiation status of the cells is regulated by two diffusible signals secreted from the cells - a short-ranged positive signal and a long-ranged negative signal, as motivated in Hiscock et al.[18]
4. A cell-based model involving cell movement and aggregation. Cells move randomly, and in response to a short-ranged chemoattractant and a long-ranged chemorepellent secreted from the cells, as motivated in Hiscock et al. [18]
5. A mechanical model based on cells migrating on and interacting with ECM, as suggested by Murray et al. [19] in the context of limb patterning.

The details of these equations follows in section S10D.

For each case, we follow the approach of Sheth et al. [4] and Raspopovic et al. [11], by considering a predominantly cubic nonlinearity in the reaction terms which reliably generates striped patterns, without having to scan through high-dimensional parameter spaces to find regimes of stripe formation. We focus on a single parameter set for each model, in which stripes are formed, but with variable direction. We then add a production gradient, a parameter gradient or an anisotropy and examine whether stripe orientation is achieved. For each case, the specific variable that is produced; or parameter that is varied; or operator that is made anisotropic is different; but in each case, the results are consistent with the simpler Swift-Hohenberg model.

S10C Previously published results are consistent with our simple model

There have been a number of existing simulation-based studies that have considered stripe orientation. In the table below, we list the model; the orientation mechanism considered; and whether the results of our analysis hold.

S10D Model equations used in figure 3

1. The CIMA system is modelled by a 2 component reaction diffusion equation[17]:

$$\frac{\partial u}{\partial t} = \nabla^2 u + a - u - 4\frac{uv}{1+u^2} \tag{S.40a}$$

$$\frac{\partial v}{\partial t} = \sigma\left(c\nabla^2 v + b\left(u - \frac{uv}{1+u^2}\right)\right) \tag{S.40b}$$

Model	Reference	Orientation mechanism	Orientation correctly predicted by SH equation?
2 component reaction-diffusion	Sheth et al. [4]	Parameter gradient	Yes, except for travelling waves
BSW model	Raspopovic et al. [11]	Parameter gradient	Yes
Reaction-diffusion model	Shoji et al. [20]	Anisotropy	Yes
Molecular model for digit patterning	Glimm et al [21]	Production gradient	Yes
Chemical Turing pattern, Brusselator	De Wit et al. [22]	Parameter gradient	Yes

We use the parameters $a = 10.2, b = 0.205, \sigma = 20, c = 1$. We incorporate production of the variable u as the production gradient, varying linearly between $[-0.01, 0.01]$; variation in parameter b as the parameter gradient, varying linearly between $[0.185, 0.265]$; and anisotropy in the diffusion of v as the anisotropy. This is captured by changing the diffusion operator to tensor form $\nabla^T \mathbf{D} \nabla$, where

$$\nabla^T \mathbf{D} \nabla \equiv \begin{pmatrix} \partial_x & \partial_y \end{pmatrix} \begin{pmatrix} D_{xx} & 0 \\ 0 & D_{yy} \end{pmatrix} \begin{pmatrix} \partial_x \\ \partial_y \end{pmatrix} \tag{S.41}$$

and we use $D_{xx} = 0.1 D_{yy}$.

2. The two component reaction-diffusion model is taken from Sheth et. al. [4]:

$$\frac{\partial}{\partial t} \begin{pmatrix} u \\ v \end{pmatrix} = \begin{pmatrix} f_U & f_V \\ g_U & g_V \end{pmatrix} \begin{pmatrix} u \\ v \end{pmatrix} + \begin{pmatrix} D_U & 0 \\ 0 & D_V \end{pmatrix} \nabla^2 \begin{pmatrix} u \\ v \end{pmatrix} - \begin{pmatrix} u^3 \\ 0 \end{pmatrix} \tag{S.42}$$

We use the parameters $f_U = 0.23, f_V = 0.5, g_U = 0.5, g_V = -0.5, D_U = 0.1, D_V = 1.25$. We use production of u as the production gradient, varying linearly from $[-0.001, 0.001]$; variation in f_U as the parameter gradient, linearly varying from $[0.20, 0.24]$ (though in fact, all 4 linear parameters can have the same effect in certain regimes, data not shown); and variation in v diffusivity as the source of anisotropy, exactly as in #1. (These parameter sets are near those defined by [4].)

3. The 3-component reaction-diffusion model is taken from Raspopovic et al. [11], the 'BSW model':

$$\frac{\partial}{\partial t} \begin{pmatrix} B \\ S \\ W \end{pmatrix} = \begin{pmatrix} -k_5 & -k_4 & 0 \\ k_2 & 0 & -k_3 \\ 0 & -k_7 & -k_9 \end{pmatrix} \begin{pmatrix} B \\ S \\ W \end{pmatrix} + \begin{pmatrix} D_B & 0 & 0 \\ 0 & 0 & 0 \\ 0 & 0 & D_W \end{pmatrix} \nabla^2 \begin{pmatrix} B \\ S \\ W \end{pmatrix} - \begin{pmatrix} 0 \\ S^3 \\ 0 \end{pmatrix} \tag{S.43}$$

Again, we focus on parameter sets used in the original study. We choose $k_2 = 1.06, k_3 = 0.7, k_4 = 1.59, h_5 = 0.1, k_7 = 1.4, k_9 = 0.1, d = 2.4, \gamma = 0.3$, where $\gamma \equiv D_W, \gamma d \equiv D_B$. We consider a production gradient of S, linearly varying between $[-0.05, 0.05]$; a parameter gradient based on k_4 linearly varying between $[1.39, 1.79]$ and using $d = 2.5, k_2 = 1.05, k_7 = 1.4$, (although other k_i gradients also apply); and anisotropy of B diffusion, exactly as in #1.

4. This cell-based model is motivated by Hiscock et al. [18]. We consider the differentiation status of a cell as a variable ϕ, and we allow cells at different points in their tissue to interact. We allow cells to interact via diffusing and linearly degrading secreted molecules, one of which is short ranged and promotes cells of the same type, A; the other is longer ranged and inhibits cells of the same type, I. These equations can be written as:

$$\frac{\partial \phi}{\partial t} = g_A(A) + g_I(I) + \lambda - \frac{\phi}{\tau} \tag{S.44}$$

$$\frac{\partial A}{\partial t} = D_A \nabla^2 A - \frac{A}{\tau_A} + f_A(\phi) \tag{S.45}$$

$$\frac{\partial I}{\partial t} = D_I \nabla^2 I - \frac{I}{\tau_I} + f_I(\phi) \tag{S.46}$$

When linearized, in the limit of rapid molecular kinetics compared to the differentiation kinetics, these equations can be mapped to the form of equations S.5 and S.6. We then choose cubic nonlinearities about the otherwise linearized set of equations, so that stripes are reliably generated, i.e.:

$$\frac{\partial \phi}{\partial t} = K * \phi - \gamma\phi - \phi^3 \tag{S.47}$$

$$K_{\mathbf{q}} \equiv \frac{h_A}{1 + L_A^2 q^2} - \frac{h_I}{1 + L_I^2 q^2} \tag{S.48}$$

We use $h_A = 1, h_I = 2, L_A = 1, L_I = 3, \gamma = 0.3$, where $\gamma \equiv 1/\tau$. We allow variation in production of ϕ as the production gradient, λ, varying linearly from $[-0.001, 0.001]$; variation in γ as an example of a parameter gradient, varying linearly from $[0.25, 0.35]$; and anisotropy in the diffusion of I, exactly as in #1.

5. A slight variant on the above model is to allow the secreted molecules to act as chemical guidance cues. The simplest representation of this case would be:

$$\frac{\partial \phi}{\partial t} = D_\phi \nabla^2 \phi - K_A \nabla.(\phi \nabla A) + K_I \nabla.(\phi \nabla I) + \lambda - \frac{\phi}{\tau} \tag{S.49}$$

$$\frac{\partial A}{\partial t} = D_A \nabla^2 A - \frac{A}{\tau_A} + f_A(\phi) \tag{S.50}$$

$$\frac{\partial I}{\partial t} = D_I \nabla^2 I - \frac{I}{\tau_I} + f_I(\phi) \tag{S.51}$$

Here, ϕ now represents density of cells. Again, we linearize this equations and allow cubic nonlinearities to straightforwardly generate stripes without having to fine tune the parameters:

$$\frac{\partial \phi}{\partial t} = D_\phi \nabla^2 \phi - \nabla^2 \left(K * \phi\right) - \gamma\phi - \phi^3 \tag{S.52}$$

We use the same parameters as above, but with $D_\phi = 0.2, \gamma = 0.1$. We use the same gradients and anisotropies as the model above. As above, we allow variation in production of ϕ as the production gradient, λ, varying linearly from $[-0.001, 0.001]$; variation in γ as an example of a parameter gradient, varying linearly from $[0.07, 0.13]$; and anisotropy in the diffusion of I, exactly as in #1.

6. The final model is a simplified version of the full Oster-Murray model used to study chondrogenesis [23, 24, 19]. It consists of a viscoelastic isotropic medium (the ECM) upon which cells migrate, exert traction forces and are passively transported (advected). The variables in this model are the ECM density, ρ, the ECM displacement, $\mathbf{u}$, and the cell density, n, with the following PDEs:

   (a) Conservation of matrix

$$\frac{\partial \rho}{\partial t} + \nabla. \left(\rho \frac{\partial \mathbf{u}}{\partial t}\right) = 0 \tag{S.53}$$

   (b) Force balance.

$$\nabla. \left[\left(\mu_1 \frac{\partial \epsilon}{\partial t} + \mu_2 \frac{\partial \theta}{\partial t} \mathbf{I}\right) + E\left(\epsilon + \nu\theta\mathbf{I}\right) + \tau\left(n + \rho + \beta\nabla^2\rho\right)\mathbf{I}\right] = -s\mathbf{u} \tag{S.54}$$

   (c) Advection of cells along the ECM

$$\frac{\partial n}{\partial t} = -\nabla. \left(n \frac{\partial \mathbf{u}}{\partial t}\right) \tag{S.55}$$

Here, $\theta \equiv \nabla.\mathbf{u}$, $2\epsilon \equiv \nabla\mathbf{u} + (\nabla\mathbf{u})^{\mathrm{T}}$ is the strain tensor, μ are viscosities, E is Young's modulus; s is an elastic restoring force exerted by attachment to an underlying substrate; τ is the traction force exerted by cells, with a nonlocal (e.g. filopodia) term captured by β. We linearize these equations, assume a cubic nonlinearity and, after rearranging, arrive at a simpler description that we simulate directly:

$$\mu \frac{\partial}{\partial t}\theta = K^{OM} * \theta - \theta^3 \tag{S.56}$$

$$K_{\mathbf{q}}^{OM} = 2\tau - E - \left(\frac{s}{q^2} + \tau\beta q^2\right) \tag{S.57}$$

Here, τ, μ, s have been rescaled by $1 + \nu$. We set $\mu = \mu_1 + \mu_2 = 1$ WLOG, and use $E = 1, s = 1, \tau = 2, \beta = 1$. We allow production of cells, adding a gradient linearly between $[-0.1, 0.1]$; variation in the Young's modulus, linearly between $[1, 1.4]$; and anisotropy of the filopodia interactions, equivalently as in #1, to orient stripes (in this case with $E = 1, s = 0.2, \tau = 0.5$ to generate similar spacing).

References

[1] Cross MC, Hohenberg PC (1993) Pattern formation outside of equilibrium. *Reviews of modern physics* 65(3):851.

[2] Gierer A, Meinhardt H (1972) A theory of biological pattern formation. *Kybernetik* 12(1):30–39.

[3] Ermentrout B (1991) Stripes or spots? nonlinear effects in bifurcation of reaction-diffusion equations on the square. *Proceedings of the Royal Society of London. Series A: Mathematical and Physical Sciences* 434(1891):413–417.

[4] Sheth R et al. (2012) Hox genes regulate digit patterning by controlling the wavelength of a turing-type mechanism. *Science* 338(6113):1476–1480.

[5] Stanojevic D, Small S, Levine M (1991) Regulation of a segmentation stripe by overlapping activators and repressors in the drosophila embryo. *Science* 254(5036):1385–1387.

[6] Hoyle R (1995) Steady squares and hexagons on a subcritical ramp. *Physical Review E* 51(1):310.

[7] Van Hecke M, Hohenberg P, Van Saarloos W (1994) Amplitude equations for pattern forming systems. *Fundamental Problems in Statistical Mechanics VIII* pp. 245–278.

[8] Pomeau Y, Zaleski S (1983) Pattern selection in a slowly varying environment. *Journal de Physique Lettres* 44(4):135–141.

[9] Kramer L, Ben-Jacob E, Brand H, Cross M (1982) Wavelength selection in systems far from equilibrium. *Physical Review Letters* 49(26):1891.

[10] Riecke H (1986) Pattern selection by weakly pinning ramps. *EPL (Europhysics Letters)* 2(1):1.

[11] Raspopovic J, Marcon L, Russo L, Sharpe J (2014) Digit patterning is controlled by a bmp-sox9-wnt turing network modulated by morphogen gradients. *Science* 345(6196):566–570.

[12] Míguez DG, Dolnik M, Muñuzuri AP, Kramer L (2006) Effect of axial growth on turing pattern formation. *Physical review letters* 96(4):048304.

[13] Averbukh I, Ben-Zvi D, Mishra S, Barkai N (2014) Scaling morphogen gradients during tissue growth by a cell division rule. *Development* 141(10):2150–2156.

[14] Crampin EJ, Gaffney EA, Maini PK (1999) Reaction and diffusion on growing domains: scenarios for robust pattern formation. *Bulletin of mathematical biology* 61(6):1093–1120.

[15] De Kepper P, Castets V, Dulos E, Boissonade J (1991) Turing-type chemical patterns in the chlorite-iodide-malonic acid reaction. *Physica D: Nonlinear Phenomena* 49(1):161–169.

[16] Lengyel I, Epstein IR (1991) Modeling of turing structures in the chlorite-iodide-malonic acid-starch reaction system. *Science* 251(4994):650–652.

[17] Lengyel I, Epstein IR (1992) A chemical approach to designing turing patterns in reaction-diffusion systems. *Proceedings of the National Academy of Sciences* 89(9):3977–3979.

[18] Hiscock TW, Megason SG (2015) Mathematically guided approaches to distinguish models of periodic patterning. *Development* 142(3):409–419.

[19] Murray J, Oster G (1984) Cell traction models for generating pattern and form in morphogenesis. *Journal of mathematical biology* 19(3):265–279.

[20] Shoji H, Iwasa Y, Mochizuki A, Kondo S (2002) Directionality of stripes formed by anisotropic reaction–diffusion models. *Journal of Theoretical Biology* 214(4):549–561.

[21] Glimm T, Zhang J, Shen YQ, Newman SA (2012) Reaction–diffusion systems and external morphogen gradients: The two-dimensional case, with an application to skeletal pattern formation. *Bulletin of mathematical biology* 74(3):666–687.

[22] De Wit A, Borckmans P, Dewel G (1993) in *Instabilities and Nonequilibrium Structures IV*. (Springer), pp. 247–258.

[23] Murray J, Oster G (1984) Generation of biological pattern and form. *Mathematical Medicine and Biology* 1(1):51–75.

[24] Murray JD, Maini P, Tranquillo R (1988) Mechanochemical models for generating biological pattern and form in development. *Physics Reports* 171(2):59–84.